

Article

Heat and Mass Transfer during Lignocellulosic Biomass Torrefaction: Contributions from the Major Components—Cellulose, Hemicellulose, and Lignin

Ken-ichiro Tanoue ^{1,*}, Kentaro Hikasa ¹, Yuuki Hamaoka ¹, Akihiro Yoshinaga ¹,
Tatsuo Nishimura ¹, Yoshimitsu Uemura ^{2,3} and Akihiro Hiden ⁴

¹ Department of Mechanical Engineering, School of Sciences and Engineering for Innovation, Yamaguchi University, Tokiwadai 2-16-1, Ube, Yamaguchi 755-8611, Japan; kentaro.hikasa@shi-g.com (K.H.); y-hamaoka@nipponpapergroup.com (Y.H.); b065vd@yamaguchi-u.ac.jp (A.Y.); tnishimu@yamaguchi-u.ac.jp (T.N.)

² NPO Kuramae Bioenergy, Minato-ku, Tokyo 108-0023, Japan; yuemura.my@gmail.com

³ Center for Biofuel and Biochemical Research, Universiti Teknologi PETRONAS, Seri Iskandar 32610, Malaysia

⁴ Paper industry innovation center of Ehime University, 127 Mendori-cho, Shkokucho 799-0113, Japan; a-hiden@agr.ehime-u.ac.jp

* Correspondence: tano@yamaguchi-u.ac.jp; Tel.: +81-836-85-9122

Received: 27 June 2020; Accepted: 6 August 2020; Published: 9 August 2020



Abstract: The torrefaction of three representative types of biomass—bamboo, and Douglas fir and its bark—was carried out in a cylindrical-shaped packed bed reactor under nitrogen flow at 573 K of the reactor wall temperature. As the thermal energy for the torrefaction was supplied from the top and the side of the bed, the propagation of the temperature profile of the bed is a crucial factor for discussing and improving the torrefaction reactor performance. Therefore, the temperature and gas flow rate (vector) profiles throughout the bed were calculated by model simulation so as to scrutinize this point. The measured temperature at a certain representative location ($z = 30$ mm and $r = 38$ mm) of the bed was well reproduced by the simulation. The volume fraction of the bed at temperatures higher than 500 K at 75 min was 0.89, 0.85, and 0.99 for bamboo, and Douglas fir and its bark, respectively. It was found that the effective thermal conductivity is the determining factor for this difference. The heat of the reactions was found to be insignificant.

Keywords: biomass torrefaction; packed bed reactor; biomass major components; reaction enthalpy; numerical simulation

1. Introduction

Biomass is one of the representative renewable energy sources, and is one of the only energy sources that is tangible, as it consists of carbon, hydrogen, oxygen, and some minor atoms. Therefore, one of the near-future applications for biomass is the production of solid fuels. Torrefaction is a promising and simple technology for producing high-quality solid fuels from biomass [1–8]. Heat transfer within biomass is an important factor for determining the performance of torrefaction, as the size of biomass in the torrefaction reactor is larger than that for the other conversion technologies, such as gasification or liquefaction.

Kinetic studies of heat and mass transfer are also being conducted experimentally and numerically regarding how much production can be expected and how much heat is required by torrefaction. A two-step parallel successive reaction model for all major components during pyrolysis, when the temperature was higher than 400 °C, has been reported by Miller et al. [9]. Their model, which was

suggested by Di Blasi (1994) [10] for cellulose pyrolysis, was extended to hemicellulose pyrolysis and lignin pyrolysis on the basis of previous experimental data. It has also been reported by Kawamoto that the cellulose of biomass is composed of crystalline (long block) and amorphous (short block) alternately, like a block co-polymer [11]. Decomposition starts at around 200 °C in the amorphous state, and the crystalline hardly decomposes at that temperature. At around 300 °C, amorphous decomposition is transmitted to the crystalline material, and the decomposition progresses rapidly.

The heat of the reactions during pyrolysis or torrefaction have been summarized in relation to the char formation [12–17]. In particular, the heat of the reactions during pyrolysis were measured directly using DSC (Differential Scanning Calorimetry), and it has been suggested that, firstly, an endothermic reaction will occur, and then an exothermic reaction will successively occur [12,14–16]. The heat of the pyrolyses of all of the major components have been reported qualitatively using DTA (differential thermal analysis) [18]. Although direct measurement by DSC for the heat of a reaction during cellulose pyrolysis was reported by Mok et al. [12], there are no data by DSC for the heat of reaction during hemicellulose pyrolysis and lignin pyrolysis. As heat and mass transfer during pyrolysis were reviewed by Di Blasi (2008) [19], it has been studied using a chemical reaction model suitable for the heat and mass transfer experimental results [20–26], and an analysis using the heat of chemical reaction commensurate with temperature change has also been conducted [20–23].

In addition, the effect of inorganic materials in biomass feedstock on torrefaction has been investigated by S. Zhang et al. [27]. They found that when the torrefaction temperature was 270 °C, the product yields for raw rice husk were 55% in char, 23% in liquid, and 21% in gas, while the product yields for rice husk with a reduced potassium concentration of less than 1 wt% of all inorganic compounds were 60% in char, 23% in liquid, and 17% in gas.

There are many varieties of biomass, but few reports have been generalized and analyzed for the thermochemical reaction of the thermal decomposition behavior, and it is not clear about heat and mass transfer in low temperature regions, like torrefaction.

In this study, we aimed to generalize the biomass torrefaction behavior using the concentrations of the major constituents of cellulose, hemicellulose, and lignin. Specifically, as shown in Figure 1, the heat of the reaction for the major components of the biomass during pyrolysis was measured. We also experimentally investigated the biomass torrefaction process on a packed bed of small particles of biomass, because a big chunk of a biomass slab is difficult to handle and has no assurance for spatial uniformity. Furthermore, the heat and mass transfer simulation during torrefaction in the biomass packed bed were performed using the heat of the chemical reaction and the pyrolysis model by Miller et al. [9]. The validity of the numerical simulation model was compared with that of the biomass torrefaction process experiment.

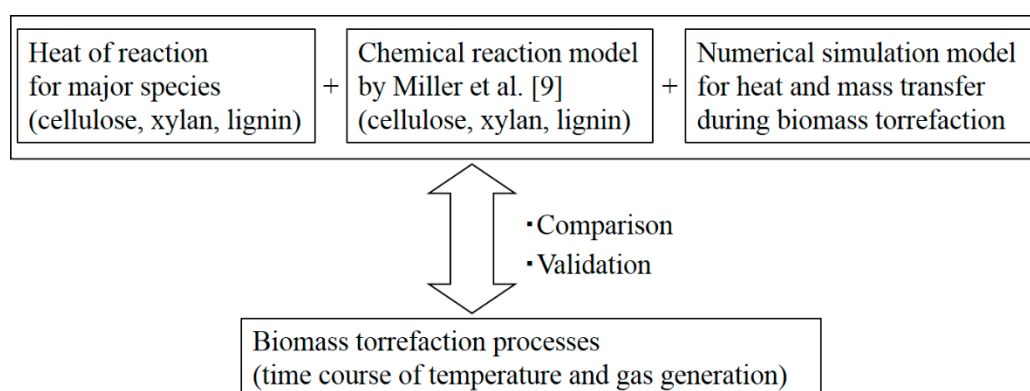


Figure 1. Concept of this work to investigate the biomass torrefaction processes.

2. Materials and Methods

2.1. Sample Preparation

Bamboo powder, Douglas fir powder, and the bark powder of Douglas fir were selected as representative biomass species. They were pulverized and sieved into #3.35 mm, #1.68 mm, #1.00 mm, and #500 μm using a motorized sieve (ANF-30, Nitto Kagaku Co., Ltd., Nagoya, Aichi, Japan). The size of about 400 particles for 500 μm or less was measured using a microscope. The constituent sugars and lignin in the bamboo and Douglas fir samples were analyzed using a modified method based on the technical report NREL/TP-510-42618 [28]. Table 1 shows the mass percentages in the major components of biomass.

Table 1. Mass percentage of major components in the biomass powder.

Biomass Species	Component (wt%)					
	Cellulose	Hemicellulose			Lignin	Others
		Xylan	Arabinan	Mannan		
Bamboo	34.1	25.2	2.3	0.2	24	14.2
Douglas fir	42.5	2.8	1.1	14	22	17.6
Bark of Douglas fir	25.4	3.3	0.9	3.9	51	15.5

Bamboo has three major components of cellulose, xylan in hemicellulose, and lignin, while Douglas fir consists of cellulose, mannan in hemicellulose, and lignin. On the other hand, there are only two major components of cellulose and lignin for the bark of the Douglas fir.

The effect of the potassium concentration in the biomass on torrefaction was also investigated, but no significant difference was found in the product yield [27]. Therefore, in this study, we investigated the effect of the cellulose, hemicellulose, and lignin concentrations on the heat and mass transfer during the biomass torrefaction.

2.2. Thermogravimetric (TG) Analysis and Differential Scanning Calorimetry (DSC)

In order to measure the heat of the reaction during the torrefaction of biomass, thermogravimetry analysis and differential scanning calorimetry analysis of pure cellulose powder (CAS RN 9004-34-6, Sigma Aldrich, Meguro-ku, Tokyo, Japan), pure xylan powder (CAS RN 9004-34-6, FUJIFILM Wako Pure Chemical Corporation, Osaka, Osaka, Japan) and pure dealkaline lignin powder (CAS RN 8068-05-1, Tokyo kasei, Chuo-ku, Tokyo, Japan) were conducted. For DSC (DSC3100s, MAC science, Chuo-ku, Tokyo, Japan) and TG (TG/DTA6300, Hitachi High-Tech Science Corporation, Minato-ku, Tokyo, Japan), the heating rate, nitrogen gas flow rate, and input mass were 10 K/min, 0.5 L/min, and 5 ± 0.25 mg, respectively. The sample sizes of the cellulose, xylan, and lignin powder were 30, 45, and 64 μm , respectively. Figure 2 shows the mass decrease profile from 300 K to 700 K from the TG analysis, as well as the relationship between the heat flow and temperature obtained by the DSC analysis for (a) cellulose, (b) xylan, and (c) lignin. The heat of reaction for these components was obtained by the following procedure.

- (1) The time or temperature of the reaction start point $t_{RS,i}$ ($T_{RS,i}$) and reaction end point $t_{RE,i}$ ($T_{RE,i}$) were decided using the trend of the DSC and TG curves.
- (2) The base line between $t_{RS,i}$ and $t_{RE,i}$ was linearly drawn in the DSC diagram.
- (3) The cross point $t_{shift,i}$ ($T_{shift,i}$) between the DSC curve and the base line was defined as the shifted point from the endothermic chemical reaction to the exothermic chemical reaction.
- (4) The endothermic and exothermic heats of reactions were given by Equations (1) and (2).

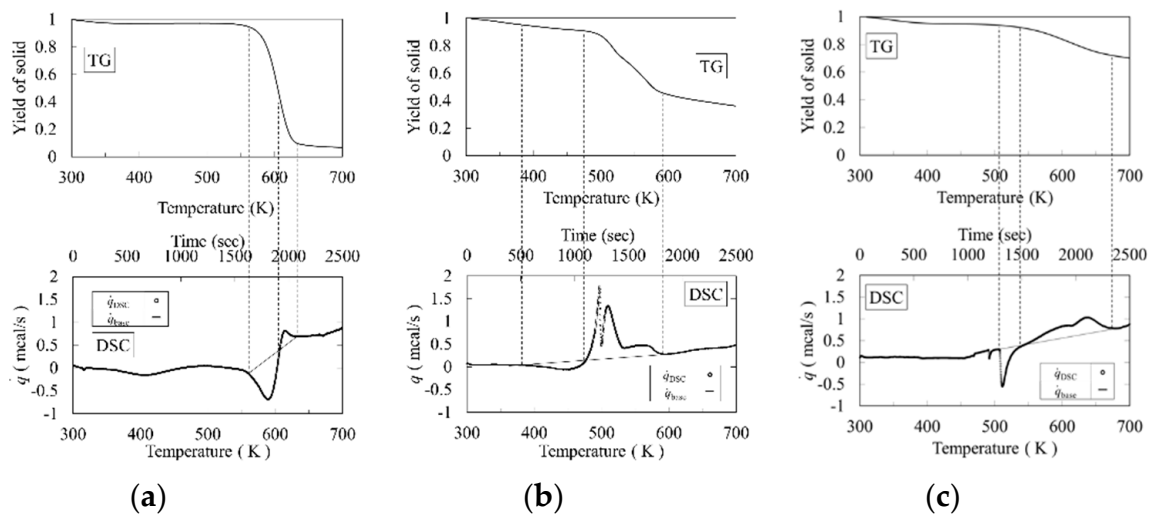


Figure 2. Results of thermogravimetry (TG) and differential scanning calorimetry (DSC) experiments. (a) Cellulose powder; (b) xylan powder; (c) lignin powder.

$$-\Delta H_{R,endo,i} = \frac{1}{m_0} \int_{t_{RS,i}}^{t_{shift,i}} (q_{base,i} - q_{DSC,i}) dt \quad (1)$$

$$-\Delta H_{R,exo,i} = \frac{1}{m_0} \int_{t_{shift,i}}^{t_{RE,i}} (q_{DSC,i} - q_{base,i}) dt \quad (2)$$

Table 2 shows the obtained heat of the reaction for cellulose pyrolysis, xylan pyrolysis, and lignin pyrolysis. From Table 2, the absolute value of the endothermic heat of the reaction was higher than that of the exothermic heat of reaction during cellulose pyrolysis, while the absolute value of the exothermic heat of reaction was higher than that of the endothermic heat of reaction during xylan pyrolysis and lignin pyrolysis.

Table 2. Results for heats of reaction during pyrolysis of major components of biomass by DSC and TG.

Component <i>i</i>	$T_{RS,i}$ (K)	$T_{RE,i}$ (K)	$T_{shift,i}$ (K)	$-\Delta H_{R,endo,i}$ (kJ/kg)	$-\Delta H_{R,exo,i}$ (kJ/kg)
Cellulose	560	638	607	-125.8	22.6
Xylan	371	602	477	-56.4	245.0
Lignin	491	682	549	-62.9	127.1

2.3. Experimental Apparatus and Procedure

The experimental apparatus is shown in Figure 3. The apparatus consisted of anitrogen gas supply, a tubular reactor, furnace, data logger, thermocouples, cold trap for tar and water, and a wet-type gas flow meter. First, 150 g of biomass powder was placed into the reactor, of which the diameter and height were 108 mm and 230 mm, respectively. N₂ gas of 0.5 standard liter per minute (SLM) was fed into the reactor so as to avoid oxidation. In addition, the temperature in the packed bed and temperature at the reactor wall were measured throughout the experiment using twelve thermocouples, and were recorded in the hard disc of a computer through a data logger. During pyrolysis, the generated moisture and tar were condensed through the stainless-steel bend pipe with a silicon tube for water cooling by the aspirator, and were trapped by the egg-plant shaped flask. The amount of generated gas during torrefaction was measured by the wet type gas meter and was recorded by the video camera. The temperature at the reactor wall was set at 573 K. Table 3 shows the experimental conditions for the biomass packed bed. Although the particles were pulverized and sieved using four sieves (#3.35mm, #1.68 mm, #1.0 mm, and #0.5 mm), the particle size differed

depending on the biomass species. In our previous research [20], we investigated the effect of the particle size on gas generation, and the maximum gas generation error was 2.4% at $D_p = 0.74$ mm and $D_p = 0.34$ mm. Therefore, for these biomass samples, this work proceeded on the assumption that the particle size dependence of the gas generation amount could be small. The biomass particles that were used were those that had been dried at 110 °C for 12 h. The bulk density depended on the type of biomass. So, the heights of the packed bed HB were also different. In consideration of the reproducibility of the total generated gas volume during the biomass torrefaction, experiments were conducted twice or more. The experimental coefficient of the validation for the total gas volume during biomass torrefaction was less than 2%.

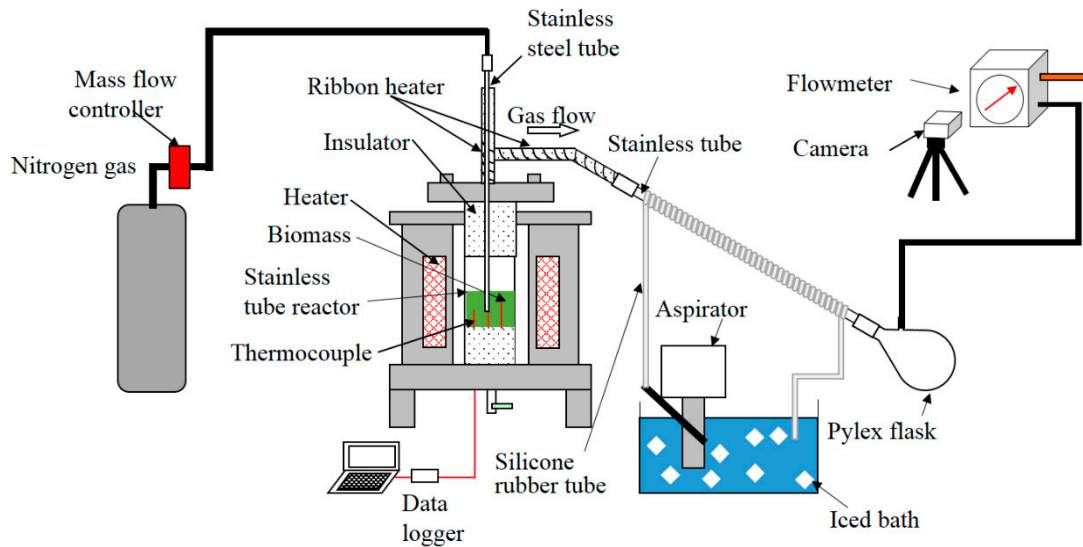


Figure 3. Experimental apparatus for measuring heat and mass transfer during the torrefaction of biomass.

Table 3. Experimental conditions of the biomass packed bed.

Biomass Species	Particle Size (μm)	Bulk Density (kg/m^3)	Height of Biomass Packed Bed, H_B (mm)
Bamboo	196	254	85
Douglas fir	317	311	68
Bark of Douglas fir	222	122	170

2.4. Numerical Simulation

The numerical simulation during pyrolysis was conducted in a two-dimensional cylindrical coordinate. Table 4 shows the governing equations for the numerical simulation. Figure 4 shows the calculation domain and boundary conditions. Although the cellulose of biomass is composed of crystalline (long block) and amorphous (short block) alternately, like a block co-polymer, as has been reported by Kawamoto [11], the co-polymer's effect of cellulose on kinetics during pyrolysis has not been investigated. In this paper, Miller's chemical reaction model and kinetic parameters during pyrolysis [9] were adapted to take into account the effect of the major components of the biomass. The pressure equation was derived from the mass balances, Ideal gas law, and Darcy's equation.

These governing equations and boundary conditions were discretized by the control volume method. In order to stabilize the numerical simulation, a hybrid scheme was adopted for the convection terms in the heat transfer and mass balances. The temperature and pressure were solved by the Euler implicit method. The material balances were solved by the fourth-order Runge–Kutta method.

The dependence of all of the physical properties on temperature was described in our previous report [24]. The change of the porosity [24–26] during torrefaction was adopted. Grid sensitivity on the time course of the temperature and generated gas flow rate were investigated using $(N_r, N_z) = (68, 102), (86, 128), (100, 149),$ and $(114, 170)$, where N_r and N_z show the mesh number along the r component and along the z component, respectively. The maximum relative error of the growth rate distributions between $(N_r, N_z) = (100, 149)$ and $(N_r, N_z) = (114, 170)$ was about 1.6%. Therefore, $(N_r, N_z) = (100, 140)$ was adopted for the bamboo torrefaction. As the heights of the packed beds were also different from the species of the biomass, $(N_r, N_z) = (100, 119)$ and $(N_r, N_z) = (100, 342)$ were adopted for the Douglas fir torrefaction and bark torrefaction, respectively.

Table 4. Chemical reaction model and governing equations of the numerical simulation during the biomass torrefaction.

Chemical Reaction Model [9]	
Energy balance	$\frac{\partial\{(\rho C)_S + \varepsilon(\rho C)_G T\}}{\partial t} + \frac{1}{r} \frac{\partial}{\partial r}(r(\rho C)_G U T) + \frac{\partial}{\partial z}((\rho C)_G W T)$ $= \frac{1}{r} \frac{\partial}{\partial r}(r \lambda_{\text{eff}} \frac{\partial T}{\partial r}) + \frac{\partial}{\partial z}(\lambda_{\text{eff}} \frac{\partial T}{\partial z}) + \sum_{i=1}^3 \sum_{j=1}^3 (R_{j,i})(-\Delta H_i)$ <p>where,</p> $(\rho C)_S = \sum_{i=1}^3 (\rho_i C_i + \rho_{\text{IM},i} C_{\text{IM},i} + \rho_{\text{Char},i} C_{\text{Char},i})$ $(\rho C)_G = \rho_{\text{N}_2} C_{\text{N}_2} + \sum_{i=1}^3 (\rho_{\text{Tar},i} C_{\text{Tar},i} + \rho_{\text{Gas},i} C_{\text{Gas},i})$ $R_{1,i} = k_{1,i} \rho_i, R_{2,i} = k_{2,i} \rho_{\text{IM},i}, R_{3,i} = k_{3,i} \rho_{\text{IM},i}$
Mass balance for component i	$\frac{d\rho_i}{dt} = -k_{1,i} \rho_i$
Mass balance for intermediate material of component i	$\frac{d\rho_{\text{IM},i}}{dt} = k_{1,i} \rho_i - k_{2,i} \rho_{\text{IM},i} - k_{3,i} \rho_{\text{IM},i}$
Mass balance for char i	$\frac{d\rho_{\text{Char},i}}{dt} = \beta_i k_{3,i} \rho_{\text{IM},i}$
Mass balance for tar i	$\frac{\partial(\varepsilon \rho_{\text{Tar},i})}{\partial t} + \frac{1}{r} \frac{\partial}{\partial r}(r \rho_{\text{Tar},i} U) + \frac{\partial}{\partial z}(\rho_{\text{Tar},i} W) = k_{2,i} \rho_{\text{IM},i} = S_{\text{Tar},i}$
Mass balance for gas i	$\frac{\partial(\varepsilon \rho_{\text{Gas},i})}{\partial t} + \frac{1}{r} \frac{\partial}{\partial r}(r \rho_{\text{Gas},i} U) + \frac{\partial}{\partial z}(\rho_{\text{Gas},i} W) =$ $(1 - \beta_i) k_{3,i} \rho_{\text{IM},i} = S_{\text{Gas},i}$
Pressure equation	$\frac{\partial(\varepsilon \frac{P}{T})}{\partial t} + \frac{1}{r} \frac{\partial}{\partial r}(r U \frac{P}{T}) + \frac{\partial}{\partial z}(W \frac{P}{T}) =$ $R_0 \left(\frac{1}{M_{\text{Tar}}} \sum_{i=1}^3 S_{\text{Tar},i} + \frac{1}{M_{\text{Gas}}} \sum_{i=1}^3 S_{\text{Gas},i} \right)$
Darcy's law	$U = -\frac{\kappa}{\mu} \frac{\partial P}{\partial r}, W = -\frac{\kappa}{\mu} \frac{\partial P}{\partial z}$

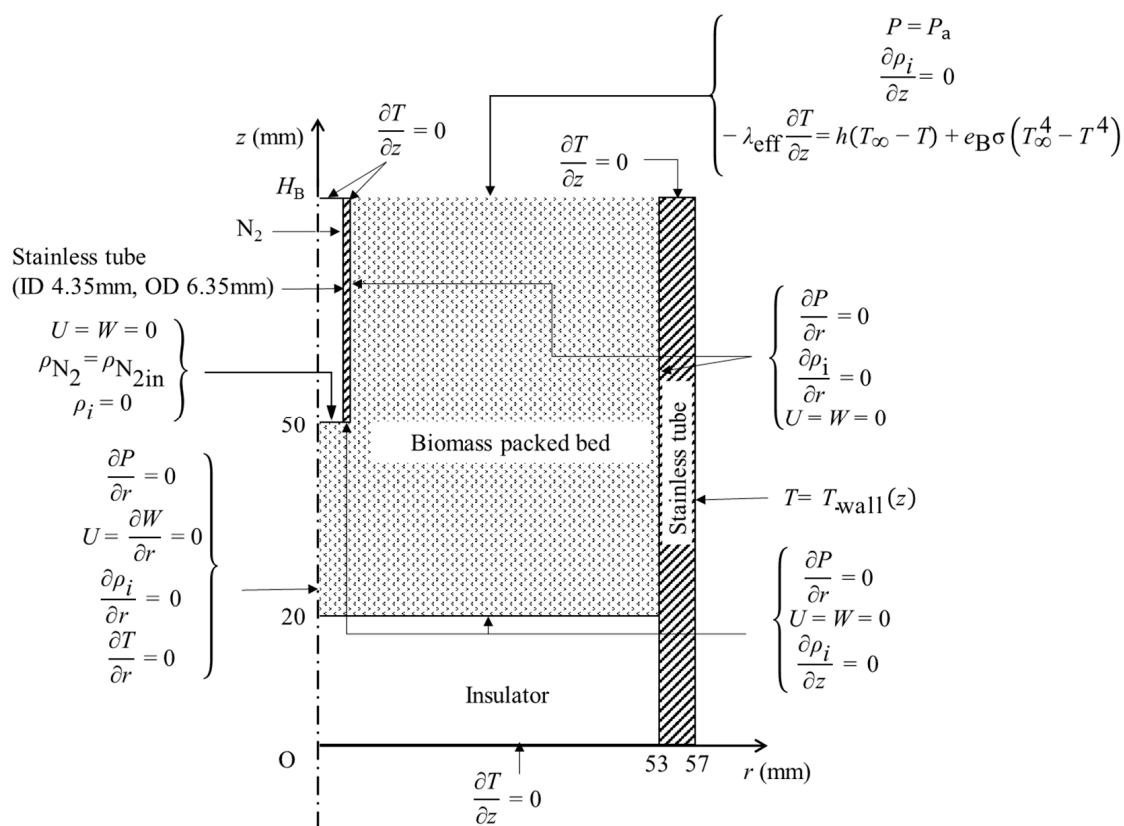


Figure 4. Boundary conditions of the numerical simulation during the biomass torrefaction.

3. Results and Discussion

3.1. Time Course of Temperature and Gas Flow Rate during Torrefaction

Figure 5 shows the time course of the temperature at $r = 38$ mm and $z = 30$ mm in the biomass packed bed and the generated gas flow rate during the biomass torrefaction. The keys and lines show the experimental results and calculation results, respectively. In Figure 5a, for the Douglas fir powder, the temperature at $r = 38$ mm and $z = 30$ mm in the bed gradually increased with time. After that, the temperature approached a constant temperature of about 573 K. The calculation temperature agreed well with the experimental one. The gas started generating at about 30 min. At $t > 40$ min, the generated gas flow rate increased adequately and had a maximum at $t = 50$ min. At this time, the temperature was $T = 450$ K, where the gas generated could be from the thermal decomposition of the mannan. After that, the gas flow rate decreased gradually with time. Although the calculation gas flow rate of the black solid line was higher than that of the experimental one, the tendency of the time course agreed quantitatively. Firstly, gas generation could be started by the hemicellulose decomposition of the green line, and had the maximum gas generation. Then, the decomposition of the lignin and the cellulose occurred. For the bamboo powder in Figure 5b, the experimental results for the time course of the temperature also agree well with the calculation results. The gas generation during the bamboo powder torrefaction was higher than that during the Douglas fir torrefaction, and could be started by the hemicellulose decomposition. Then, as the decomposition of the lignin and cellulose occurred, the gas generation had a quasi-state value and decreased with time. For the bark of the Douglas fir powder in Figure 5c, the experimental results for the time course of the temperature also agree well with the calculation results. The maximum gas generation during the bark of the Douglas fir powder torrefaction was higher than that during the Douglas fir torrefaction, and could be started by the lignin decomposition. Then, as the decomposition of the hemicellulose and cellulose occurred successively, the gas generation had a quasi-state value and decreased with time. The total

generated gas of the bark of the Douglas fir torrefaction was lower than that of the bamboo powder torrefaction. Therefore, it was found that the time course of the temperature and gas generation during the torrefaction of the biomass depended strongly on the mass percentage of the major components.

From Figure 5, the numerical calculation result of the gas generation flow rate during torrefaction was higher than the experimental one for all of the biomass species. Although the Miller model has been compared with the experimental results of several biomasses in a temperature range of 400 °C or higher [9], there are no data using Miller's reaction model in the low temperature range of 300 °C. It is also necessary to study the heat transfer and gas generation behavior of cellulose, lignin, and hemicellulose, which are the major components of biomass at around 300 °C. Furthermore, it is necessary to reexamine the pyrolysis model with reference to Di Blasi's experiment [29], regarding the reaction rate constants k_2 and k_3 of the second step in the Miller model [9].

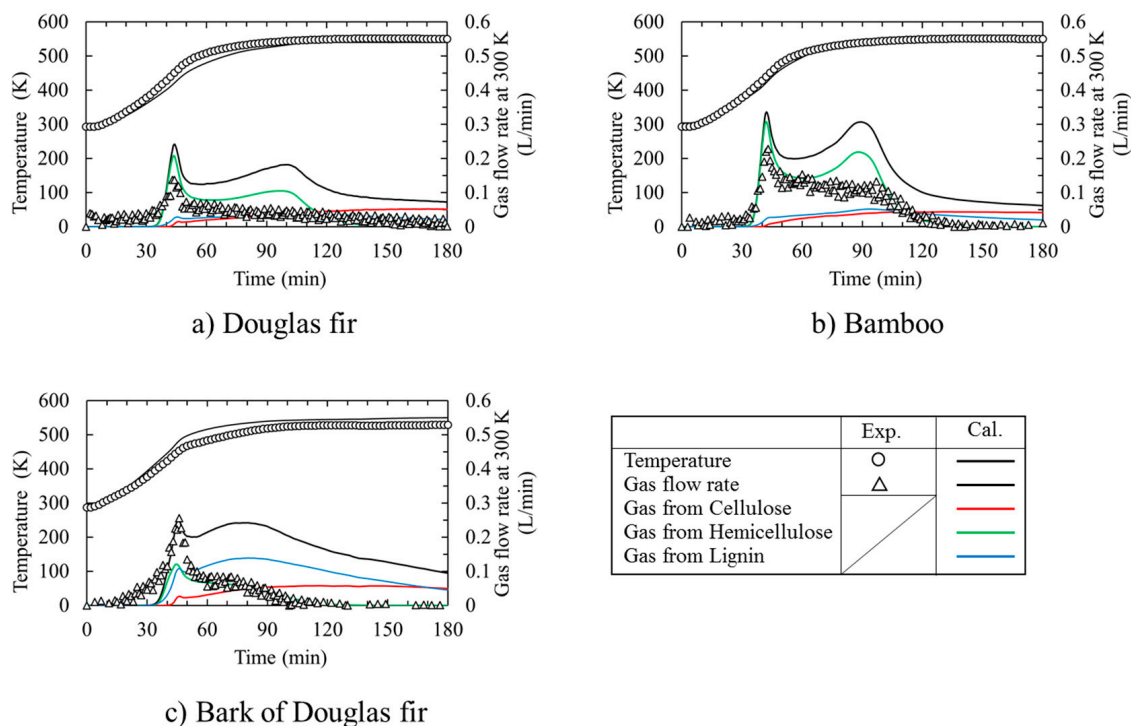


Figure 5. Time course of the temperature and generated gas flow rate during the biomass torrefaction.

3.2. Heat and Mass Transfer during Torrefaction of Biomass

Figure 6 shows the calculation results for the special profile of the temperature, gas flow velocity vector (left), and the solid density (SD, right) at different reaction times. The rectangular blank at the top center in the right figure represents a stainless-steel pipe. The temperature of the bed rose from the top and left, which means the side wall, with the torrefaction time. The zone for temperatures higher than 540 K started prevailing (volume fraction = 0.83) at 180 min. Together with the high temperature zone propagation, the local SD of the bed became smaller with a similar profile. Surprisingly, the decrease in SD propagation was not as significant as the temperature propagation in the bed. In other words, the decrease in SD propagation showed a certain time delay of 60 to 90 min in comparison with the temperature profile propagation. This may be related to the sweep gas flow profile, time required for completing the reaction, or the difference between primary decomposition (k_1) and secondary decomposition (k_2 and k_3) in the bed. In order to clarify this point of "what caused this delay?", further investigation is required. At $t = 30$ min, the heat transfer due to the thermal conduction occurred from the reactor wall, and at the top surface of the backed bed, the temperature at the center and bottom region was less than 400 K. No torrefaction occurred at 30 min. At $t = 60$ min, as the temperature at the wall and top surface of the packed bed was higher than 500 K, decomposition started from the corner

of the top surface. With the passing of time, the temperature near the region of the packed bed was higher than 500 K, the decomposition was propagated. At $t = 180$ min, the Douglas fir packed bed at the region of the top and near the wall decomposed to about 70% of the initial packed bed, while the Douglas fir packed bed at the other region could not be pyrolyzed.

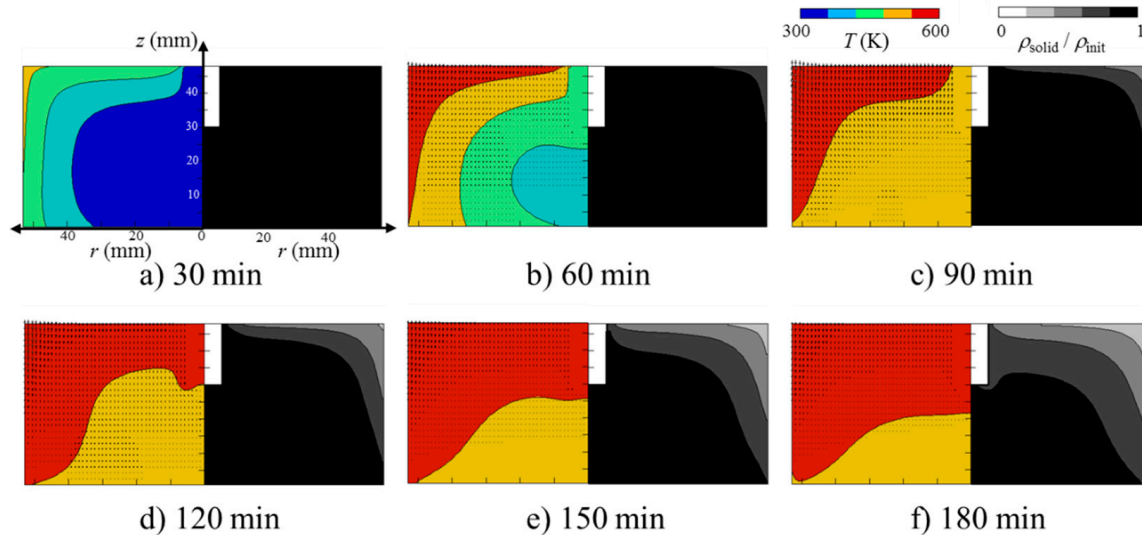


Figure 6. Calculation results for the time course of the temperature, velocity vectors, and total solid distribution during Douglas fir powder torrefaction. $\rho_{\text{init}} = 353 \text{ kg/m}^3$.

Figure 7 shows the calculation results for the heat and mass transfer at 75 min during various biomass torrefactions. As shown in Figure 6b for the bamboo powder torrefaction, the temperature in the packed bed was higher than that for the Douglas fir torrefaction, due to the bulk density. Furthermore, as the highest mass percentage of the major component in the bamboo was xylan, the decomposition rate in the bamboo packed bed was higher than that in the Douglas fir packed bed. As shown in Figure 6c for the bark of the Douglas fir powder torrefaction, the temperature in the packed bed was also higher than that for the Douglas fir torrefaction, because of the bulk density. However, as the most greatest percentage of the major component in the bark of Douglas fir was lignin, the decomposition rate was higher than that in the Douglas fir packed bed. The volume fraction of the bed at temperatures higher than 500 K at 75 min was 0.89, 0.85, and 0.99 for bamboo, and Douglas fir and its bark, respectively. It was found that the effective thermal conductivity was the determining factor for this difference, because the effective thermal conductivity of the bed at temperatures higher than 540 K at 75 min was 0.0254, 0.0252, and 0.0303 W/(m² K) for bamboo, and Douglas fir and its bark, respectively. Overall, the bamboo torrefaction was the highest in this study.

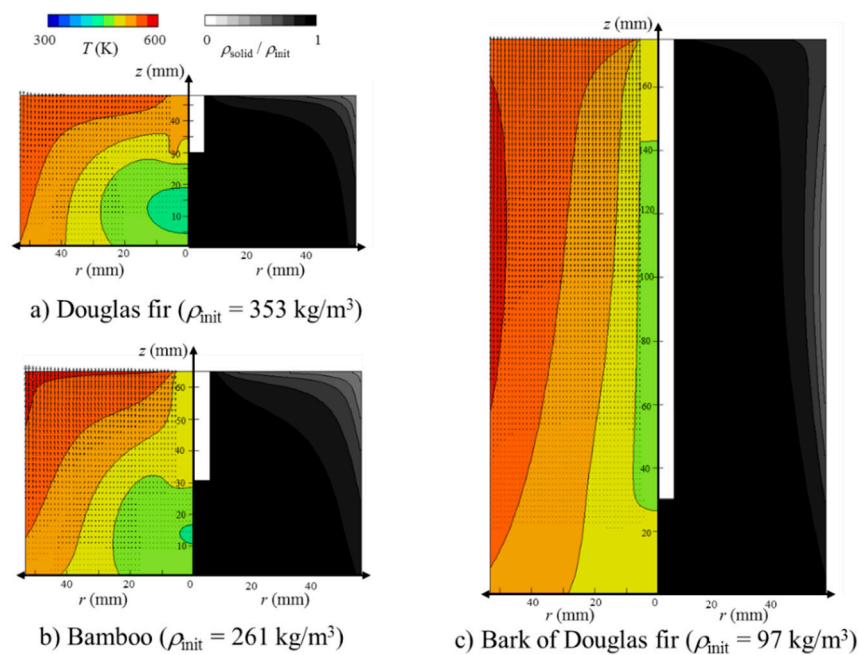


Figure 7. Calculation results for temperature, velocity vectors and solid distributions at 75 min during torrefaction for various kinds of biomass.

4. Conclusions

In this study, the torrefaction of three representative types of biomass, namely, bamboo, and Douglas fir and its bark, was carried out experimentally and numerically, paying attention to the concentrations of the major constituents of cellulose, hemicellulose, and lignin in a cylindrical-shaped packed bed reactor under a nitrogen flow at 573 K of the reactor wall temperature. The following conclusions were obtained.

- (1) From DSC experiments, the cellulose pyrolysis was progressed mainly by endothermic reaction (s) while xylan pyrolysis and lignin pyrolysis were proceeded mainly by exothermic reaction (s).
- (2) Hemicellulose decomposition could be occurred firstly during Douglas fir torrefaction and bamboo torrefaction. And then lignin and cellulose decomposition would be occurred. So, a quasi-state gas flow rate could be observed. On the other hand, bark of Douglas fir torrefaction depends strongly on the lignin decomposition.
- (3) The time course of the temperature in the packed bed agreed well with that of the calculation by taking into account the heat of reaction for not only the Douglas fir, but also for bamboo and the bark of Douglas fir. On the other hand, the numerical calculation result of the gas generation flow rate during torrefaction was higher than the experimental one for all of the biomass species, because there are no data using Miller's reaction model [9] in the low temperature range of 300 °C. It is also necessary to study the heat transfer and gas generation behavior of cellulose, lignin, and hemicellulose, which are the major components of biomass at around 300 °C. Furthermore, it is necessary to reexamine the pyrolysis model with reference to Di Blasi's experiment [29] regarding the reaction rate constants k_2 and k_3 of the second step in the Miller model [9].
- (4) The zone at temperatures higher than 540 K prevailed (volume fraction = 0.83) at 180 min. Together with the high temperature zone propagation, the local SD of the bed became smaller with a similar profile. Surprisingly, the decreased solid density (SD) propagation was not as significant as the temperature propagation in the bed. In other words, the SD decrease propagation showed a certain time delay of 60 to 90 min in comparison with the temperature profile propagation. This may be related to the sweep gas flow profile, time required for completing the reaction, or the difference between primary decomposition (k_1) and secondary decomposition (k_2 and k_3)

in the bed. In order to clarify this point of “what caused this delay?”, further investigation is required. As the temperature at the wall and top surface of the packed bed was higher than 500 K, the decomposition started from the corner of the top surface. With the elapsed time, the temperature near the region of the packed bed was higher than 500 K, and the decomposition was propagated. At $t = 180$ min, the Douglas fir packed bed at the region of the top and near the wall decomposed to about 70% of the initial packed bed, while the Douglas fir packed bed at the other region could not be pyrolyzed.

- (5) For the bamboo powder torrefaction, the temperature in the packed bed was higher than that for the Douglas fir torrefaction because of the bulk density. Furthermore, as the greatest mass percentage of the major component in the bamboo was xylan, the decomposition rate in the bamboo packed bed was higher than that in the Douglas fir packed bed. As the greatest mass percentage of the major component in the bark of Douglas fir was lignin, the decomposition rate was higher than that in the Douglas fir packed bed. The volume fraction of the bed at temperatures higher than 500 K at 75 min was 0.89, 0.85, and 0.99 for bamboo, and Douglas fir and its bark, respectively. It was found that the effective thermal conductivity was the determining factor for this difference, because the effective thermal conductivity of the bed at temperatures higher than 540 K at 75 min was 0.0254, 0.0252, and 0.0303 W/(m² K) for bamboo, and Douglas fir and its bark, respectively. Overall, the bamboo torrefaction was the highest in this study.

Author Contributions: Conceptualization, K.-i.T. and K.H.; methodology, K.-i.T. and Y.H.; software, K.-i.T.; validation, A.Y. and Y.U.; formal analysis, K.-i.T., K.H., and A.H.; investigation, K.H., Y.H., A.Y., and A.H.; resources, A.H.; data curation, K.H., Y.H., A.Y., and A.H.; writing (original draft preparation), K.-i.T.; writing (review and editing), K.-i.T. and Y.U.; visualization, A.Y.; supervision, T.N. and Y.U.; project administration, K.-i.T.; funding acquisition, T.N. All authors have read and agreed to the published version of the manuscript.

Funding: This work was supported, in part, by a Grant-in Aid for Scientific Research C (no. 17K06196) from the Japan Society for the Promotion of Science.

Acknowledgments: Special thanks to Toshihide Irii and Hamza Bin Rahim for preparing the experimental equipment.

Conflicts of Interest: The authors declare no conflict of interest.

Nomenclature

C	Heat capacity (J/(kg K))
e	Emissivity
H_B	Height of biomass packed bed (m)
h	Heat transfer coefficient between biomass and gas (W/(m ² K))
$\Delta H_{R,endo,i}$	Endothermic heat of reaction during pyrolysis of biomass major component i (J/kg)
$\Delta H_{R,exo,i}$	Exothermic heat of reaction during pyrolysis of biomass major component i (J/kg)
i	Major component i of biomass ($i =$ cellulose, hemicellulose, and lignin)
$k_{1,i}, k_{2,i}, k_{3,i}$	Reaction rate constant in Miller’s chemical reaction model for component i [9] (1/s)
M_{Tar}	Molecular weight of tar (= 0.11 kg/mol [22])
M_{Gas}	Molecular weight of gas (= 0.38 kg/mol [22])
m_0	Input mass of TG and DSC experiments (kg)
N	Maximum grid number
P	Pressure (Pa)
q_{base}	Heat flow of the base line from the endothermic chemical reaction to the exothermic chemical reaction (J/s)
q_{DSC}	Heat flow in DSC curve (J/s)
R_i	Reaction rates in Miller’s chemical reaction model for component i [9] (kg/(m ³ s))
R_0	Universal gas constant (= 8.314 J/(mol K)) (J/(mol K))
r	r coordinate in the packed bed (mm)
S_{Tar}	Reaction rate of tar for component i (kg/(m ³ s))
S_{Gas}	Reaction rate of gas for component i (kg/(m ³ s))

T	Temperature (K)
$T_{RS,i}$	Temperature at reaction start time in TG curve for component i (K)
$T_{RE,i}$	Temperature at reaction end time in TG curve for component i (K)
$T_{shift,i}$	Temperature at the shifted time from the endothermic chemical reaction to the exothermic chemical reaction in TG curve for component i (K)
$t_{RS,i}$	Reaction start time in TG curve for component i (s)
$t_{RE,i}$	Reaction end time in TG curve for component i (s)
$t_{shift,i}$	Shifted time from the endothermic chemical reaction to the exothermic chemical reaction in the TG curve for component i (s)
U	Volume averaged Darcy's velocity along the r -axis in the packed bed (m/s)
W	Volume averaged Darcy's velocity along the z -axis in the packed bed (m/s)
z	z coordinate in the packed bed (mm)
<i>Greek symbol</i>	
β_i	kinetic parameter in Miller's chemical reaction model for component i [9]
ε	Porosity in the packed bed
κ	Permeability in the packed bed (m^2)
λ	Thermal conductivity (W/(mK))
μ	Viscosity (Pa s)
ρ	Density (kg/m^3)
σ	Stefan–Boltzman constant ($= 5.669 \times 10^{-8} W/m^2K^4$) (W/m^2K^4)
<i>Subscript</i>	
a	Atmosphere
Char	Char
eff	Effective
Gas	Gas
im	Intermediate material
init	Initial value
N_2	Nitrogen
r	r component
s	Solid
Tar	Tar
v	Volatile
wall	Wall of the stainless-steel tube
z	z component
∞	Environmental condition on the wall of the stainless-steel tube

References

1. Hisam, S.M.; Uemura, Y.; Tazli, A.M. Effects of Temperature and Concentration of Oxygen on Torrefaction of Empty Fruit Bunches. *J. Jpn. Inst. Energy* **2016**, *95*, 1110–1114.
2. Yoshida, T.; Kubojima, Y.; Kamikawa, D.; Kiguchi, M.; Tanaka, K.; Miyago, M.; Masui, M.; Ohyabu, Y.; Kobayashi, A.; Igarashi, H. Production Test of Torrefied Woody Biomass Solid Fuel in an Original Small-scale Plant. *J. Jpn. Inst. Energy* **2018**, *97*, 231–235. [[CrossRef](#)]
3. Chen, W.H.; Chen, J.; Peng, J.; Bi, X.T. A state-of-the-art review of biomass torrefaction, densification and applications. *Renew. Sustain. Energy Rev.* **2015**, *44*, 847–866. [[CrossRef](#)]
4. Ribeiro, J.M.C.; Godina, R.; Matias, J.C.D.O.; Nunes, L.J.R. Future perspectives of biomass torrefaction: Review of the current state-of-the-art and research development. *Sustainability* **2018**, *10*, 2323. [[CrossRef](#)]
5. Rodrigues, A.; Loureiro, L.; Nunes, L.J.R. Torrefaction of woody biomasses from poplar SRC and Portuguese roundwood: Properties of torrefied products. *Biomass Bioenergy* **2018**, *108*, 55–65. [[CrossRef](#)]
6. Nunes, L.J.; Matias, J.C. Biomass Torrefaction as a Key Driver for the Sustainable Development and Decarbonization of Energy Production. *Sustainability* **2020**, *12*, 922. [[CrossRef](#)]
7. Loureiro, L.M.; Nunes, L.J.; Rodrigues, A.M. Woody biomass torrefaction: Fundamentals and potential for Portugal. *Silva Lusit.* **2017**, *25*, 35–63.

8. Filipe dos Santos Viana, H.; Martins Rodrigues, A.; Godina, R.; Carlos de Oliveira Matias, J.; Jorge Ribeiro Nunes, L. Evaluation of the physical, chemical and thermal properties of Portuguese maritime pine biomass. *Sustainability* **2018**, *10*, 2877. [[CrossRef](#)]
9. Miller, R.S.; Bellan, J. A Generalized Biomass Pyrolysis Model Based on Superimposed Cellulose, Hemicellulose and Lignin Kinetics. *J. Comb. Sci. Tech.* **1997**, *126*, 97–137. [[CrossRef](#)]
10. Di Blasi, C. Numerical simulation of cellulose pyrolysis. *Biomass Bioenergy* **1994**, *7*, 87–98. [[CrossRef](#)]
11. Kawamoto, H. Reactions and molecular mechanics of cellulose pyrolysis. *Mokuzai Gakkaishi* **2015**, *61-1*, 1–24. [[CrossRef](#)]
12. Mok, W.S.L.; Antal, M.J., Jr. Effects of pressure on biomass pyrolysis. II. Heats of reaction of cellulose pyrolysis. *Thermochimica Acta* **1983**, *68*, 165–186. [[CrossRef](#)]
13. Milosavljevic, I.; Oja, V.; Suuberg, E.M. Thermal Effects in Cellulose Pyrolysis: Relationship to Char Formation Processes. *Ind. Eng. Chem. Res.* **1996**, *35*, 653–662. [[CrossRef](#)]
14. Ratha, J.; Wolfinger, M.G.; Steinera, G.; Krammera, G.; Barontinib, F.; Cozzanib, V. Heat of wood pyrolysis. *Fuel* **2003**, *82*, 81–91. [[CrossRef](#)]
15. Gomez, C.; Velo, E.; Barontini, F.; Cozzani, V. Influence of Secondary Reactions on the Heat of Pyrolysis of Biomass. *Ind. Eng. Chem. Res.* **2009**, *48*, 10222–10233. [[CrossRef](#)]
16. Joungmo, C.; Jeffrey, M.D.; George, W.H. The Intrinsic Kinetics and Heats of Reactions for Cellulose Pyrolysis and Char Formation. *ChemSusChem* **2010**, *3*, 1162–1165.
17. Richard, B.B.; Ahmed, F.G. Biomass torrefaction: Modeling of reaction thermochemistry. *Bioresour. Technol.* **2013**, *134*, 331–340.
18. Yang, H.; Yan, R.; Chen, H.; Lee, D.H.; Zheng, C. Characteristics of hemicellulose, cellulose and lignin pyrolysis. *Fuel* **2007**, *86*, 1781–1788. [[CrossRef](#)]
19. Di Blasi, C. Modeling chemical and physical processes of wood and biomass pyrolysis. *Prog. Ener. Comb. Sci.* **2008**, *34*, 47–90. [[CrossRef](#)]
20. Pyle, D.L.; Zaror, C.A. Heat transfer and kinetics in the low temperature pyrolysis of solids. *Chem. Eng. Sci.* **1984**, *39-1*, 147–158. [[CrossRef](#)]
21. Koufopoulos, C.A.; Papayannakos, N. Modelling of the Pyrolysis of Biomass Particles. Studies on Kinetics, Thermal and Heat Transfer Effects. *Can. J. Chem. Eng.* **1991**, *69*, 908–915. [[CrossRef](#)]
22. Won, C.P.; Arvind, A.; Howard, R.B. Experimental and theoretical investigation of heat and mass transfer processes during wood pyrolysis. *Combust. Flame* **2010**, *157*, 481–494.
23. Okekunle, P.O.; Pattanotai, T.; Watanabe, H.; Okazaki, K. Numerical and Experimental Investigation of Intra-Particle Heat Transfer and Tar Decomposition during Pyrolysis of Wood Biomass. *J. Therm. Sci. Technol.* **2011**, *6*, 360–375. [[CrossRef](#)]
24. Tanoue, K.; Suetomi, T.; Nishimura, T.; Taniguchi, M.; Sasauchi, K. Thermal conduction and gas generation undergoing pyrolysis in the packed bed of woody biomass. *J. Jpn. Inst. Energ.* **2012**, *91*, 976–984. (In Japanese) [[CrossRef](#)]
25. Tanoue, K.; Suetomi, T.; Uemura, Y.; Nishimura, T.; Taniguchi, M.; Sasauchi, K. Effect of Tar Decomposition On Gas Generation During Pyrolysis in Packed Bed of Woody Biomass. *Int. J. Biomass Renew.* **2013**, *2*, 1–6.
26. Tanoue, K.; Hamaoka, Y.; Nishimura, T.; Taniguchi, M.; Sasauchi, K. Influence of Volume Shrinkage and Water Evaporation on Heat Transfer and Chemical Reactions During the Pyrolysis of A Cellulose-Powder-Packed Bed. *Int. J. Biomass Renew.* **2018**, *7*, 1–16.
27. Zhang, S.; Su, Y.; Ding, K.; Zhu, S.; Zhang, H.; Liu, X.; Xiong, Y. Effect of inorganic species on torrefaction process and product properties of rice husk. *Bioresour. Technol.* **2018**, *265*, 450–455. [[CrossRef](#)]
28. Sluiter, A.; Hames, B.; Scarlata, R.C.; Sluiter, J.; Templeton, D.; Crocker, D. Determination of structural carbohydrates and lignin in biomass. *Lab. Anal. Proced.* **2008**, *1617*, 1–16.
29. Di Blasi, C.; Lanzetta, M. Intrinsic kinetics of isothermal xylan degradation in inert atmosphere. *J. Anal. Appl. Pyrolysis* **1997**, *40*, 287–303. [[CrossRef](#)]

